ADAPTIVE CLUTCH PRESSURE CONTROL FOR TRACTOR POWERSHIFT TRANSMISSION BASED ON THE FFDL-MFAC ALGORITHM

/

基于 FFDL-MFAC 算法的拖拉机动力换挡变速箱离合器压力自适应控制

Ruqi TANG [1)], Wen ZHANG[1,2)], Ruixin LAN[1)], Naixu REN[1)], Xinzhe ZHANG[1)], Shenghui FU [*1,2)]
[1)] College of Mechanical and Electronic Engineering, Shandong Agricultural University, Taian 271018 / China;
[2)] Shandong Engineering Research Center of Agricultural Equipment Intelligentization, Taian 271018 / China;
Tel: +8618811126208; E-mail: fush@sdau.edu.cn; Corresponding author: Shenghui FU
DOI: https://doi.org/10.35633/inmateh-78-90

Keywords: *tractor; wet clutch; model free adaptive control; improved mayfly algorithm*

ABSTRACT

To address the challenges of strong nonlinearity, time-varying parameters, and significant external disturbances in wet clutch pressure control during tractor powershift operation, this study proposes an adaptive pressure control method based on Full-Form Dynamic Linearization Model-Free Adaptive Control (FFDL-MFAC). Sobol global sensitivity analysis is employed to identify the key controller parameters, and an Improved Mayfly Algorithm (IMA) is introduced to achieve global optimization. The controller performance is evaluated through co-simulation and hardware-in-the-loop (HIL) testing. The co-simulation results show that, compared with conventional PID control, the FFDL-MFAC controller reduces the rise and fall times in square-wave tracking from 2.63 s and 1.27 s to 0.72 s and 0.52 s, respectively, achieving fully monotonic responses without overshoot or undershoot. In sinusoidal tracking, the maximum pressure error decreases from 0.036 MPa to 0.021 MPa, while the response delay is reduced from 0.07 s to less than 0.005 s. HIL-based clutch pressure control experiments further verify the effectiveness of the optimized controller when implemented on real hardware. Compared with the PID controller, which exhibits a 9.44% overshoot, a settling time of 3.12 s, and a steady-state fluctuation of 0.40 MPa, the FFDL-MFAC controller shows no noticeable overshoot, shortens the settling time to 1.24 s, and maintains minimal steady-state fluctuation. These results confirm the effectiveness and superiority of the proposed method for wet clutch pressure regulation and provide a solid foundation for high-performance control in tractor powershift transmissions.

摘要

针对拖拉机动力换挡过程中湿式离合器压力控制存在的非线性强、参数时变及受外部扰动影响显著等问题，本文提出一种基于全格式无模型自适应控制（Full-Form Dynamic Linearization Model-Free Adaptive Control, FFDL-MFAC）的离合器压力自适应控制方法。本文采用 Sobol 全局灵敏度分析筛选控制器关键参数，并引入改进蜉蝣算法（Improved Mayfly Algorithm, IMA）进行全局优化。通过联合仿真与硬件在环（HIL）试验对控制器性能进行验证。联合仿真结果表明，与 PID 控制相比，FFDL-MFAC 在方波压力跟随中将上升与下降段的调节时间分别由 2.63s、1.27s 降至 0.72s、0.52s，响应单调无超调或欠调；在正弦跟随中，最大压力误差由 0.036MPa 降至 0.021MPa，响应延时由 0.07s 降至 0.005s 内。HIL 离合器压力控制试验进一步验证了优化控制器在真实硬件执行下的有效性。与存在 9.44%超调、3.12s 调节时间及 0.40MPa 稳态波动的 PID 控制相比，FFDL-MFAC 无明显超调，将调节时间降低至 1.24s，稳态波动极小。研究结果验证了该方法在湿式离合器压力控制中的有效性与优越性，为拖拉机动力换挡过程的高性能控制提供基础。

INTRODUCTION

With the continuous development of tractors toward higher power, faster speed, lower energy consumption, and greater intelligence, powershift technology has become essential for improving operational performance and driving comfort. As the core actuator of the powershift transmission system, the wet clutch directly determines the smoothness of gear shifting and drivetrain reliability *(Cvok et al., 2024; Wang et al., 2025; Zhou et al., 2018*). Its hydraulic system is a highly nonlinear electro-hydraulic-mechanical coupling system affected by parameter fluctuations, hydraulic lag, oil temperature variation, and external disturbances, often leading to slow dynamic response and limited control accuracy. Thus, achieving fast, precise, and adaptive clutch pressure control remains a key challenge in powershift research *(Li et al., 2023; Walker et al., 2011; Zhao et al., 2021*).

Traditional PID and its variants feature simple structures and easy implementation but struggle to balance response speed and steady-state accuracy under nonlinear and strongly disturbed conditions *(Han et al., 2019; Zhang et al., 2022*).

To enhance performance, *(Meng et al., 2015),* developed a feedforward–feedback hybrid control strategy using turbine speed variation for real-time adjustment, while *Jung et al., (2020),* designed an adaptive feedforward controller to reduce control delay. *Song & Sun, (2011),* applied a sliding mode control approach combined with an observer for online estimation of clutch piston displacement. Although these methods improved dynamic performance, their effectiveness depends on accurate system models. However, the wet clutch hydraulic system is inherently nonlinear and time-varying, making precise modeling difficult.

Model-Free Adaptive Control (MFAC) eliminates the need for an explicit mathematical model, achieving adaptive regulation through input–output data with strong real-time adaptability and robustness *(Xin et al., 2025; Zhu & Hou, 2013*). The Full-Form Dynamic Linearization MFAC (FFDL-MFAC) algorithm further enhances dynamic representation and pseudo-gradient estimation accuracy, but its multi-parameter tuning process still faces issues such as computational complexity, slow convergence, and local optima *(Mi et al., 2025; Xiong et al., 2020*). Intelligent optimization algorithms, known for global search and high efficiency, have been widely adopted for controller parameter tuning (*Duan et al., 2024; Feng et al., 2021; Hasan et al., 2023*). For instance, *Yuan et al., (2025),* used the Hummingbird Optimization Algorithm for adaptive controller tuning, and *Zhao et al., (2025),* introduced an improved Northern Goshawk Optimization algorithm for active disturbance rejection control, achieving enhanced tracking performance and stronger disturbance rejection..

In this study, an FFDL-MFAC-based clutch pressure controller is developed. Sobol global sensitivity analysis is employed to identify key controller parameters, and the Improved Mayfly Algorithm (IMA) is applied for global optimization. Hardware-in-the-Loop (HIL) experiments verify the superior performance of the proposed method in wet clutch pressure control.

MATERIALS AND METHODS

Modeling of the Hydraulic System of a Wet Clutch

The wet clutch system in the tractor powershift transmission mainly comprises the transmission control unit (TCU), wet clutch, oil pump, proportional pressure-reducing valve, relief valve, and related hydraulic components, as shown in Figure 1. The proportional valve includes a pilot valve, solenoid coil, main spool, return spring, and valve body. During clutch engagement, the TCU energizes the solenoid coil, generating electromagnetic force that drives the pilot spool to restrict the outlet flow, thereby increasing the pilot chamber pressure. This pressure shifts the main spool rightward, allowing hydraulic oil to enter the clutch cylinder until an equilibrium is established among the pilot, feedback, and spring forces. When disengaging, the solenoid is de-energized, hydraulic oil is discharged to the reservoir, and the main spool returns under spring force, completing the release process.

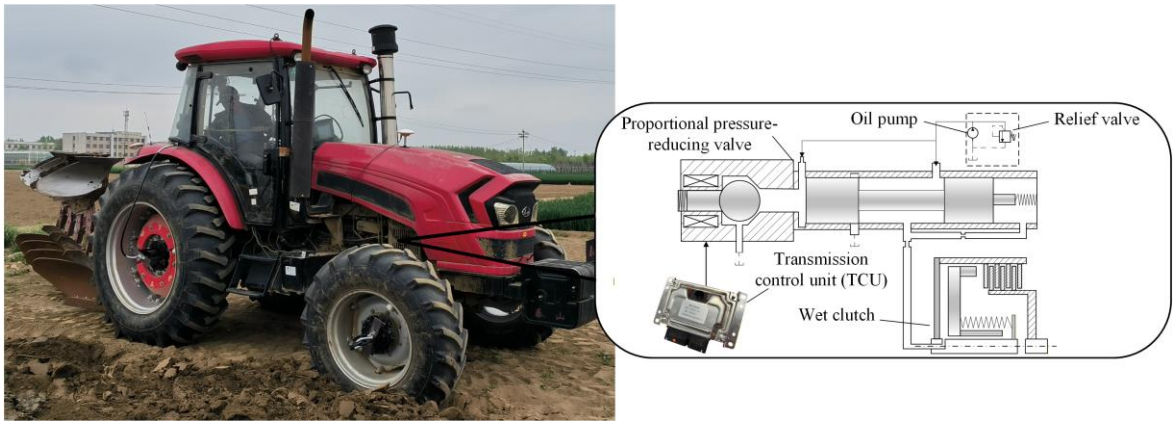

Fig. 1 - Schematic Diagram of the Wet Clutch System

Model of the Proportional Pressure-Reducing Valve

(1) Force Equilibrium Equation of the Pilot Valve Spool.

$$m_{sv}\ddot{x}_{sv} + B_{sv}\dot{x}_{sv} + k_{sv}\left(x_{sv} + x_{sv0}\right) + F_{sv} = F_{mag} - \frac{\pi d_{sv}^2}{4}\left(P_{vc} - P_{v0}\right) \quad (1)$$

where, m_{sv} is mass of the pilot valve spool, kg; B_{sv} is viscous damping coefficient of the pilot valve spool, N·s/m; F_{mag} is electromagnetic force, N; x_{sv} is displacement of the pilot valve spool, m; x_{sv0} is initial compression of the pilot valve spring; F_{sv} is steady-state hydraulic force acting on the pilot valve spool, N; d_{sv} is diameter of the pilot valve inlet port, m; P_{vc} is control chamber pressure, MPa; P_{v0} is return passage pressure, MPa.

(2) Force Equilibrium Equation of the Main Valve Spool

$$m_v\ddot{x}_v + B_v\dot{x}_v + K_s(x_{v0}+x_v) + F_v = \frac{\pi d_v^2}{4}\left(P_{svc} - P_{vf}\right) \tag{2}$$

$$F_v = \begin{cases} -2C_{dv}C_v A_e x_v \cos(\theta_v)(P_v - P_{v0}), \\ \quad 0 \le x_v < h_v \\ 0, \qquad h_v \le x_v \le (h_v + h_d) \\ 2C_{dv}C_v A_i x_v \cos(\theta_v)(P_s - P_v), \\ \quad (h_v + h_d) < x_v \le x_{vm} \end{cases} \tag{3}$$

$$A(d,x) = \frac{d^2}{4}\left[\arccos\left(1-\frac{2x}{d}\right) - 2\left(1-\frac{2x}{d}\right)\sqrt{\frac{x}{d}-\left(\frac{x}{d}\right)^2}\right] \tag{4}$$

$$A_e(x_v) = n_v A(d, h_v - x_v), 0 \le x_v \le h_v \tag{5}$$

$$A_s(x_v) = n_v A(d, x_v - h_v - h_d), x_v > h_v + h_d \tag{6}$$

where, m_v is mass of the main valve spool, kg; B_v is viscous damping coefficient of the main valve spool, N·s/m; x_{v0} is initial compression of the main spool spring, m; x_v is displacement of the main valve spool, m; F_v is steady-state hydraulic force acting on the main valve spool, N; P_{vf} is pressure in the main valve feedback chamber, N; K_s is main spool spring stiffness, N·m^{-1}; C_{dv} is flow coefficient of the main valve orifice; C_v is velocity coefficient of the main valve orifice; A_e is flow area of the main valve outlet port, m^2; A_i is flow area of the main valve inlet port, m^2; A is flow area of the orifice-type throttle, m^2; d is diameter of the orifice-type throttle, m; x is opening displacement of the orifice-type throttle, m; θ_v is jet angle of the main valve orifice, rad; P_v is output pressure of the proportional valve, MPa; h_v is initial opening of the main valve outlet port, m; h_d is initial overlap of the main valve inlet port, m.

(3) Pilot valve pressure–flow equation

$$q_{sv} = C_{dsv}A_{si}(x_{sv})\sqrt{\frac{2}{\rho}(P_{svc} - P_{v0})} \tag{7}$$

where, q_{sv} is flow rate through the pilot valve orifice, m^3/s; C_{dsv} is flow coefficient of the pilot valve orifice; ρ is density of the hydraulic oil, kg/m^3; A_{si} is flow area of the pilot valve orifice, m^2;

(4) Main valve pressure–flow equation

$$q_v = \frac{C_{dvc}\pi d_{vc}^2}{4}\sqrt{\frac{2}{\rho}(P_s - P_{vc})} \tag{8}$$

$$q_{vf} = sign(P_v - P_{vf})\frac{C_{dvf}\pi d_{vf}^2}{4}\sqrt{\frac{2}{\rho}(P_v - P_{vf})} \tag{9}$$

$$q_v = \begin{cases} -C_{dv}A_e x_v\sqrt{\frac{2}{\rho}(P_v - P_{v0})}, & 0 \le x_v < h_v \\ 0, & h_v \le x_v \le (h_v + h_d) \\ C_{dv}A_e x_v\sqrt{\frac{2}{\rho}(P_s - P_v)}, & (h_v + h_d) < x_v \le x_{vm} \end{cases} \tag{10}$$

where, q_v is flow rate through the damping orifice of the control chamber, m^3/s; C_{dvc} is flow coefficient of the control chamber orifice; P_s is supply pressure of the hydraulic system, MPa; d_{vc} is diameter of the damping orifice in the control chamber, m; q_{vf} is flow rate through the damping orifice of the feedback chamber, m^3/s; C_{dvd} is flow coefficient of the feedback chamber orifice; d_{vf} is diameter of the damping orifice in the feedback chamber, m; P_{vf} is pressure of the feedback chamber, MPa; q_v is flow rate through the proportional valve, m^3/s.

(5) Flow Continuity Equation of the Feedback Chamber

The hydraulic fluid entering the feedback chamber through the inlet port is partly utilized to compensate for the oil compressibility, while the remaining portion counteracts the variation in the feedback chamber volume induced by the motion of the main valve spool. The flow behavior can be expressed by the following continuity equation:

$$\dot{P}_{vf} = \frac{\beta_e}{V_{vf}} \cdot \left(q_{vf} + \frac{\pi d_v^2}{4} \dot{x}_v \right) \tag{11}$$

where, V_{vf} is the volume of the feedback chamber, m³; β_e is the effective bulk modulus of the hydraulic oil, MPa.

(6) Flow Continuity Equation of the Main Chamber

$$\dot{P}_v = \frac{\beta_e}{V_v} \cdot \left(q_v - q_{vc} + q_{vf} \right) \tag{12}$$

where, V_v is the volume of the main chamber, m³; q_{vc} is the clutch filling flow rate, m³/s.

(7) Force Equilibrium Equation of the Clutch Piston

The wet clutch engagement process comprises rapid filling, slipping, and compression stages. The piston motion is driven mainly by hydraulic pressure and resisted by spring and sealing forces; torque transfer begins in the slipping phase and rigid coupling is established after full compression.

$$\ddot{x}_{vc} m_{vc} + \beta_{vc} \dot{x}_{vc} = P_{vc} A_{vc} + F_\omega - F_{se} - K_{vc} x_{vc} - F_{vc0} - F_{vc} \tag{13}$$

Here: $F_{se} = 2\psi_{se} b_s P_{vc} \pi \left(R_1 + R_2 \right)$; $F_{vc} = K_n \left(x_{vc} - \Delta \right) \quad (x_{vc} > \Delta)$; $F_\omega = \frac{\pi \rho}{4} \left(\alpha_\omega \omega \right)^2 \left(R_2^2 - R_1^2 \right) \left(R_2^2 + R_1^2 - 2R_o^2 \right)$

where, x_{vc} is displacement of the clutch piston, m; β_{vc} is viscous damping coefficient of the piston, N·s/m; P_{vc} is clutch pressure, MPa; A_{vc} is effective area of the piston, m²; F_ω is centrifugal hydraulic force acting on the piston, N; F_{se} is frictional force of the piston sealing ring, N; K_{vc} is stiffness of the return spring, N/m; F_{vc0} is preload force of the return spring, N; F_{vc} is compressive force on the friction plates, N; ψ_{se} is friction coefficient of the piston sealing ring; b_s is width of the piston sealing ring, m; R_1 is inner radius of the piston, m; R_2 is outer radius of the piston, m; K_n is equivalent stiffness of the friction plates, N/m; Δ is displacement corresponding to the friction plate kiss point, m; α_ω is lag coefficient; ω is angular velocity of the clutch cylinder, rad/s; R_o is rotational radius of the clutch oil inlet passage, m.

(8) Clutch Pressure–Flow Equation

$$q_{vc} = \text{sign}\left(P_v - P_{vc} \right) C_{dv} A_{vci} \sqrt{\frac{2}{\rho} \left(P_v - P_{vc} \right)} \tag{14}$$

where, A_{vci} is the inlet port area of the clutch cylinder, m².

(9) Clutch Flow Continuity Equation

$$\dot{P}_{vc} = \frac{\beta_e \left(q_{vc} - A_{vc} \dot{x}_{vc} \right)}{V_{vc}} \tag{15}$$

where, V_{vc} is the volume of the clutch cylinder, m³.

Design of FFDL-MFAC Clutch Pressure Controller

The wet clutch pressure control system can be abstracted as the following single-input single-output nonlinear discrete-time system.

$$y(k+1) = f\left(y(k), \cdots, y(k - n_y), u(k), \cdots u(k - n_u) \right) \tag{16}$$

Where, $u(k)$ is the proportional pressure-reducing valve input voltage at time k; $y(k)$ is the clutch cylinder pressure at time k; n_y and n_u are the unknown output order of clutch pressure and input order of control voltage, respectively; $f(\ )$ is an unknown nonlinear function

The following standard assumptions are made for the full-form nonlinear discrete-time system:

Assumption 1: For the variables $u(k)$,⋯, $u(k\text{-}L_u\text{+}1)$, the function $f(\ )$ has continuous first-order partial derivatives.

Assumption 2: The system satisfies the generalized Lipschitz condition, that is, for any $k_1 \neq k_2$, if k_1, $k_2 \geq 0$ and $\boldsymbol{H}_{L_y,L_u}(k) \neq \boldsymbol{H}_{L_y,L_u}(k)$ are given, then:

$$\left| y(k_1 + 1) - y(k_2 + 1) \right| \leq b \left\| \boldsymbol{H}_{L_y,L_u}(k_1) - \boldsymbol{H}_{L_y,L_u}(k_2) \right\| \tag{17}$$

where, $y(k_i\text{+}1)\text{=}f(y(k_i),\ldots,y(k_i\text{-}n_y),u(k_i),\ldots,u(k_i\text{-}n_u))$, $i\text{=}1,2$; $b\text{>}0$ is a constant; $\boldsymbol{H}_{L_y,L_u}(k)$ is the historical data vector of the proportional pressure-reducing valve input voltage and clutch cylinder pressure, with a dimension of $L_y\text{+}L_u$, where L_y and L_u denote the pseudo-orders of the system output and input, respectively.

When Assumptions 1 and 2 hold, and $\left\|\Delta H_{L_y,L_u}(k)\right\| \neq 0$, there exists a bounded pseudo-gradient vector $\boldsymbol{\phi}_{f,Ly,Lu}(k)$, such that the system can be transformed into the FFDL model:

$$\Delta y(k+1) = \boldsymbol{\phi}^T_{f,L_y,L_u}(k)\Delta \boldsymbol{H}_{L_y,L_u}(k) \tag{18}$$

Where, $\Delta y(k+1)$ is output increment, $\Delta y(k+1) = y(k+1) - y(k)$; $\boldsymbol{\phi}_{f,Ly,Lu}(k)$ is pseudo-gradient vector, $\phi_{f,L_y,L_u}(k) = \left[\phi_1(k),\ldots,\phi_{L_y}(k),\phi_{L_y+1}(k),\phi_{L_y+L_u}(k)\right]^T$; $\Delta H_{Ly.Lu}(k)$ is input-output increment vector, $\Delta H_{L_y,L_u}(k) = [\Delta y(k),\cdots,\Delta y(k-L_y+1),\Delta u(k),\cdots,\Delta u(k-L_u+1)]^T$.

Within the FFDL-based clutch pressure model, the proportional valve input $u(k)$ is optimized for precise pressure tracking. A weighted one-step prediction error cost function is then formulated to balance tracking speed and control smoothness:

$$J(u(k)) = \left|y^*(k+1) - y(k+1)\right|^2 + \lambda\left|u(k) - u(k-1)\right|^2 \tag{19}$$

where, λ is weighting coefficient.

Substituting Equation (18) into Equation (19) and taking the partial derivative with respect to $u(k)$, the optimal control law of the proportional pressure-reducing valve can be obtained as:

$$u(k) = u(k-1) + \frac{\rho_{L_y+1}\phi_{L_y+1}(k)\left(y^*(k+1) - y(k)\right)}{\lambda + \left|\phi_{L_y+1}(k)\right|^2} - \frac{\phi_{L_y+1}(k)\sum_{i=1}^{L_y}\rho_i\phi_i(k)\Delta y(k-i+1)}{\lambda + \left|\phi_{L_y+1}(k)\right|^2} - \frac{\phi_{L_y+1}(k)\sum_{i=L_y+2}^{L_y+L_u}\rho_i\phi_i(k)\Delta u(k-L_y-i+1)}{\lambda + \left|\phi_{L_y+1}(k)\right|^2} \tag{20}$$

where, ρ_i is step factor, $\rho_i \in (0,1]$, i=1, 2,⋯, L_y+L_u

The pseudo-gradient vector $\boldsymbol{\phi}_{f,Ly,Lu}(k)$ in the FFDL model is time-varying and cannot be calibrated offline. In this study, an adaptive update algorithm based on the projection concept is adopted. This method relies solely on input and output data and can iteratively refine the pseudo-gradient while maintaining manageable computational complexity.

To ensure the stability and convergence of the estimation process, the following performance index function is introduced:

$$J(u(k)) = \left|y(k) - y(k-1) - \phi^T_{f,L_y,L_u}(k)\Delta H_{L_y,L_u}(k-1)\right|^2 + \tau\left\|\phi_{f,L_y,L_u}(k) - \hat{\phi}_{f,L_y,L_u}(k-1)\right\|^2 \tag{21}$$

where, τ is penalty weighting factor, τ>0.

By performing optimality analysis on the above equation, the iterative update formula of the pseudo-gradient can be obtained as:

$$\hat{\phi}_{f,L_y,L_u}(k) = \hat{\phi}_{f,L_y,L_u}(k-1) + \frac{\tau\Delta H_{L_y,L_u}(k-1)\,y(k) - y(k-1)}{\tau + \left\|\Delta H_{L_y,L_u}(k-1)\right\|^2} - \frac{\eta\Delta H_{L_y,L_u}(k-1)\phi^T_{f,L_y,L_u}(k-1)\Delta H_{L_y,L_u}(k-1)}{\tau + \left\|\Delta H_{L_y,L_u}(k-1)\right\|^2} \tag{22}$$

where, η is step-size factor, $\eta \in (0,2]$

Controller Parameter Tuning Based on the Improved Mayfly Algorithm

In the FFDL-MFAC clutch pressure controller, control performance is influenced by multiple parameters, including the step factors in the control law, parameters related to pseudo-gradient estimation, and initial value settings. Direct high-dimensional global optimization of all parameters can easily lead to the curse of dimensionality, resulting in low optimization efficiency and poor convergence. Therefore, this study introduces the Sobol global sensitivity analysis method to identify key parameters and employs the Improved Mayfly Algorithm (IMA) to optimize them. The output pseudo-gradient order is set to L_y=3, and the input pseudo-gradient order to L_u=2. The parameters to be optimized include λ, ρ_1, ρ_2, ρ_3, ρ_4, ρ_5, μ, η, and the initial pseudo-gradient values $\phi_1(0)$, $\phi_2(0)$, $\phi_3(0)$, $\phi_4(0)$ and $\phi_5(0)$.

Global Sensitivity Analysis Based on the Sobol Method

The Sobol global sensitivity analysis method is based on the variance decomposition theory, which decomposes the performance index function $f(\boldsymbol{X})$ into the sum of individual parameter effects and their interaction terms. By calculating the contribution ratio of each parameter to the total variance of the performance index, the method quantifies the influence of each parameter on control performance:

$$f(\boldsymbol{X}) = f_0 + \sum_{i=1}^{n} f_i(x_i) + \sum_{1\le i\le j\le n}^{n} f_{ij}(x_i, x_j) + \cdots + f_{1,2,\cdots,n}(x_1, x_2, \cdots, x_n) \quad (23)$$

where, $\boldsymbol{X}$ is random vector composed of 13 controller parameters to be tuned, $\boldsymbol{X}$=(λ, ρ_1, ρ_2, ρ_3, ρ_4, ρ_5, μ, η, $\phi_1(0)$, $\phi_2(0)$, $\phi_3(0)$, $\phi_4(0)$, $\phi_5(0)$; f_0 is expectation of $f(x)$; $f_i(x_i)$ is first-order effect term; $f_{ij}(x_i,x_j)$ is second-order interaction effect term; n_d is number of parameters to be tuned, n_d=13; $f_{1,2,\ldots,n}(x_1,x_2,\ldots,x_{nb})$ is n_d-order interaction effect.

Based on the decomposition in Eq. (23), the total variance of the model can be expressed as:

$$V(Y) = \sum_{i=1}^{n_d} V_i + \sum_{i}^{n_d}\sum_{i<j}^{n_d} V_{ij} + \cdots + V_{1,2,\cdots,n_d} \quad (24)$$

where, V_i is the variance contribution of the i-th parameter acting individually; V_{ij} is the variance contribution of the interaction between two parameters.

By transforming Eq. (24), the following expression is obtained:

$$1 = \sum_{i}^{n_d} S_i + \sum_{i}^{n_d}\sum_{i<j}^{n_d} S_{ij} + \cdots + S_{1,2,\cdots,n_d} \quad (25)$$

where, S_i is the first-order Sobol sensitivity index; S_{ij} is the second-order Sobol sensitivity index; $S_{1,2,\ldots,nd}$ is the n_d - th order sensitivity index.

The total Sobol sensitivity index S_{Ti} can be obtained by summing all orders of Sobol sensitivity indices as follows:

$$S_{Ti} = S_i + \sum_{j\ne i}^{n_d} S_{ij} + \sum_{\substack{j,k\ne i \\ j<k}}^{n_d} S_{ij} + \cdots + S_{1,2,\cdots,n_d} \quad (26)$$

Improved Mayfly Algorithm

Lens Imaging-Based Reverse Learning Strategy

To enhance the algorithm's global search capability, a lens imaging-based reverse learning strategy is introduced to increase population diversity and expand coverage of unexplored solution spaces. The lens imaging-based reverse learning strategy is an optimization approach inspired by the optical characteristics of convex lens imaging. By generating rotational points of original solutions within the solution space, the search range of the population is expanded and its diversity is enhanced. The behavior of mayflies identifying rotational points in the space is modeled as the imaging process of a convex lens. Assume that within the interval [lb,ub], there exists an individual P with a height h, and its projection on the X-axis is denoted as X, (where X represents the global optimal solution). The reference point O is defined as the midpoint of the interval, and a convex lens with focal length F is placed at this point. After passing through the convex lens, the individual P forms an inverted image P* with a height h* and a projection on the X-axis denoted as X*. According to the principle of convex lens imaging, the following relationship can be obtained:

$$\frac{(ub+lb)/2 - X}{X^* - (ub+lb)/2} = \eta \quad (27)$$

where, η is the scaling factor, η=h/h^*.

From Equation (27), the reverse point can be obtained as:

$$X^* = \frac{ub+lb}{2} + \frac{ub+lb}{2\cdot\eta} - \frac{X}{\eta} \quad (28)$$

By adjusting the scaling factor η, the reverse solution can be dynamically varied, thereby enhancing the algorithm's local exploitation capability.

Lévy Mutation Disturbance Strategy

To prevent some individuals from falling into evolutionary stagnation, the Lévy mutation strategy is applied to perturb mayfly individuals trapped in local optima, thereby enhancing population diversity and improving the algorithm's ability to escape stagnation during iterations. The Lévy mutation strategy originates from the Lévy flight mechanism, which simulates the random walk pattern of albatross foraging. The step length follows a Lévy distribution, effectively enhancing the algorithm's global search capability in complex solution spaces and avoiding local optima.

The Lévy mutation strategy can be expressed as:

$$L_v(\alpha) = \frac{\zeta}{|v|^{\alpha^{-1}}} \tag{29}$$

where, α is distribution index; ζ and v is Gaussian random variables, $\zeta \sim N\left(0, \sigma_u^2\right)$ and $v \sim N(0,1)$; σ_u is scale parameter determined by α, $\sigma_u = \left(\frac{\Gamma(1+\alpha)\sin(\pi\alpha/2)}{2^{2/(\alpha-1)}\alpha\Gamma\left((1+\alpha)/2\right)} \right)^{1/\alpha}$; $\Gamma(\cdot)$ is Gamma function.

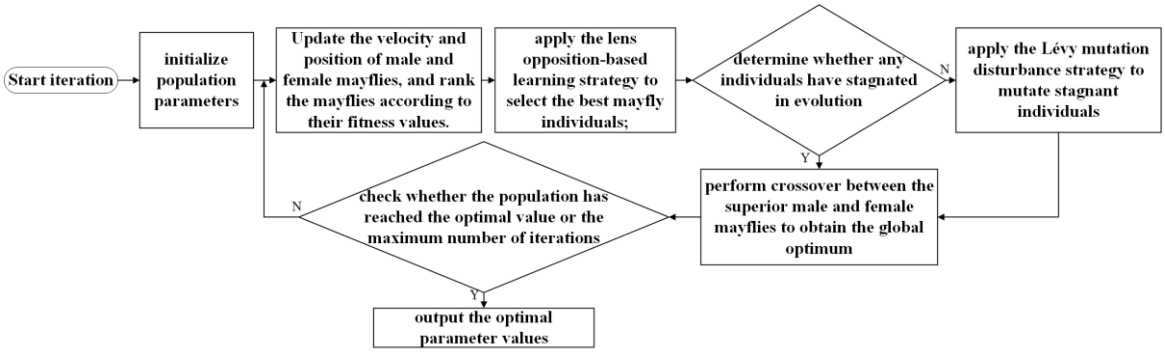

Fig. 2 - Improved mayfly algorithm process

Controller Parameter Tuning Procedure

To facilitate computation, the parameter tuning of the FFDL-MFAC controller was formulated as a penalty-based unconstrained optimization problem, as expressed by:

$$\min J(\theta) = \sum_{k=1}^{T} [y(k) - y^*(k)]^{\mathrm{T}} [y(k) - y^*(k)] + \beta_1 P_a + \beta_2 P_p \tag{30}$$

where, $y^*(k)$ denote the target clutch pressures, respectively. The first term represents the cumulative tracking error, while P_a, P_p are smooth "positive-part" penalty functions corresponding to actuator limits and pressure safety boundaries respectively; β_1 and β_2 are weighting coefficients.

Based on this formulation, the Sobol global sensitivity analysis was used to quantify the influence of each controller parameter on $J(\theta)$. Parameters with higher total sensitivity indices were then selected for optimization. The Improved Mayfly Algorithm (IMA) was employed to minimize Eq.(30) The optimization iterated until convergence, and the parameter set yielding the minimum objective value was adopted as the optimal configuration for subsequent validation.

Hardware-in-the-Loop Simulation Platform for Clutch Pressure Control

Traditional bench tests involve complex hydraulic setups, leading to high cost and testing risk. With Hardware-in-the-Loop (HIL) technology, real controllers can interact with real-time simulation models, enabling rapid and low-risk validation of clutch pressure control strategies. A HIL platform combining an AMESim hydraulic actuator model, a Simulink-based control algorithm, and a physical TCU was developed on the NI PXIe-1082 VeriStand system, as illustrated in Fig.3. The HIL setup consists of an NI PXIe-1082 chassis, an EVPT VCU3000-P36 TCU, and a host computer. Analog control signals are conditioned through an SCB-68A interface card and forwarded to the PXIe-1082, where the compiled AMESim model is executed in real time as a DLL. The key actuator parameters used in the experiments are summarized in Table 1.

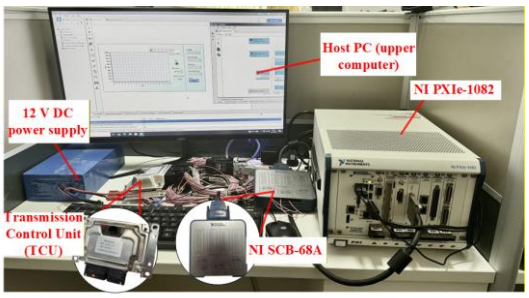

Fig. 3 - Hardware-in-the-loop test platform

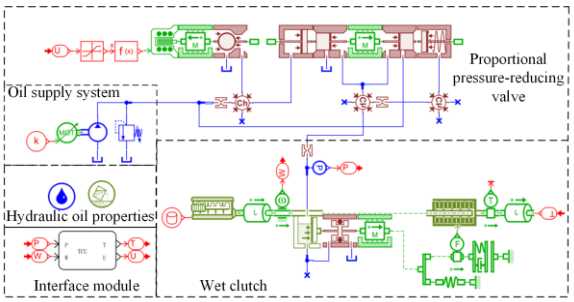

Fig. 4 - Simulation model of the wet clutch actuator

Table 1

Main parameters of the proportional pressure-reducing valve and the clutch

Parameter	Value	Parameter	Value
Supply pressure, Ps, [MPa]	2	Mass of the main valve spool, mv, [kg]	0.015
Density of the hydraulic oil, ρ, [kg·m^{-3}]	860	Mass of the pilot valve spool, msv, [kg]	0.018
Effective bulk modulus of the hydraulic oil, βe, [MPa]	1.7× 109	Stiffness of the main spool spring, Ks, [N·m^{-1}]	2000
Inlet flow area of the pilot chamber, Asi, [m²]	1.96× 10-7	Equivalent stiffness of the friction plates, Kn, [N·m^{-1}]	1.6134 ×108
Inlet flow area of the feedback chamber, Avf, [m²]	1.96× 10-7	Displacement corresponding to the friction plate kiss point, Δ, [m]	0.004
Inlet port area of the clutch cylinder, Avc, [m²]	1.96× 10-5	Initial compression of the main spool spring, xv0, [m]	0.001
Mass of the piston, mvc, [kg]	0.65	Stiffness of the pilot valve spring, kp, [N·m^{-1}]	1000
Stiffness of the piston return spring Kvc, [N·m^{-1}]	104500	Preload force of the piston return spring, Fvc0, [N]	3094
Radius of the pilot valve spool, rp, [m]	0.0026	Diameter of the throttling orifice, d, [m]	0.003
Outer radius of the piston, R2, [m]	0.07	Inner radius of the piston, R1, [m]	0.035

RESULTS AND DISCUSSIONS

Controller Parameter Sensitivity Analysis and Optimization Tuning Results

Within the specified parameter bounds, Sobol sequence sampling generated $N\times(n_d+2)$ sets (where N=500, 7,500 total samples). The controller was executed for each set to compute the performance index. As shown in Fig. 5, parameters λ, η, and ρ_1 exhibited the most significant influence on system performance, with total sensitivity indices all exceeding 0.3. The initial pseudo-gradient value $\phi_1(0)$ had an S_{Ti} of 0.221, indicating relatively high sensitivity as well. The parameters ρ_2, ρ_3, ρ_4, ρ_5, μ, $\phi_2(0)$, $\phi_3(0)$, $\phi_4(0)$, and $\phi_5(0)$ had S_{Ti} values below 0.2, and were classified as less sensitive parameters. Therefore λ, η, ρ_1 and $\phi_1(0)$ were selected as the key sensitive parameters to be tuned for the controller.

The Improved Mayfly Algorithm (IMA) was applied to minimize $J(\theta)$. with a population of 50 and 300 iterations, terminating when fitness improvement fell below 10^{-4} for 10 generations. As shown in Fig. 6, the IMA converged to J=0.60 after 143 iterations, while the baseline MA required 179 iterations, demonstrating faster convergence and higher optimization accuracy. The optimal controller parameters obtained from the IMA were λ=0.18, η=1.20, ρ_1=0.34, and $\phi_1(0)$=1.10.

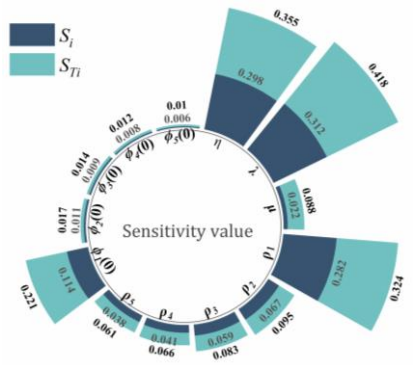

Fig. 5 - Sensitivity analysis results

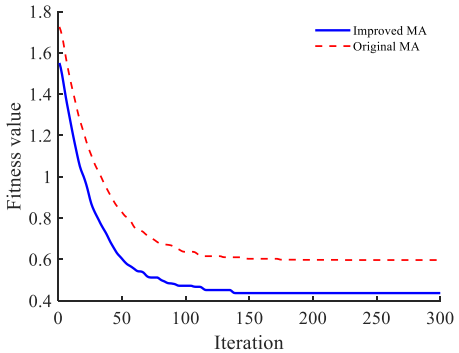

Fig. 6 - Fitness curve

Results of the Clutch Pressure Control Simulation

To comprehensively evaluate the proposed FFDL-MFAC algorithm, the verification workflow was first carried out in a co-simulation environment. This stage aimed to isolate the controller behavior from hardware and hydraulic nonlinearities, thereby assessing its intrinsic tracking capability under idealized actuator dynamics. Two representative tests were conducted: square-wave pressure tracking and sinusoidal tracking (Figs. 7 and 8). These tests emulated the repeated pressure rise and fall occurring during periodic gear shifting and allowed quantitative evaluation of tracking accuracy, response speed, and dynamic consistency.

Square-wave pressure tracking test

A 20s square-wave pressure-tracking test was conducted, as shown in Fig. 7a. The target pressure was 1 MPa during 0–2 s and 7–10 s, and 1.8 MPa during 2–7 s. At the 2 s rising step, both controllers followed the pressure increase, but their transient responses differed. Using the ±2% band, the adjustment times of PID and FFDL-MFAC were 2.63 s and 0.72 s, respectively. PID produced a 4.11% overshoot and persistent oscillations, whereas the FFDL-MFAC output rose monotonically with no overshoot. During the 7 s pressure drop, the adjustment times were 1.27 s and 0.52 s, and PID exhibited a 3.56% undershoot, while FFDL-MFAC showed none and achieved a smoother descent. The steady-state errors were −0.013 MPa for PID and negligible for FFDL-MFAC (on the order of 10^{-4} MPa). Overall, FFDL-MFAC delivered superior transient behavior and much lower steady-state error than PID.

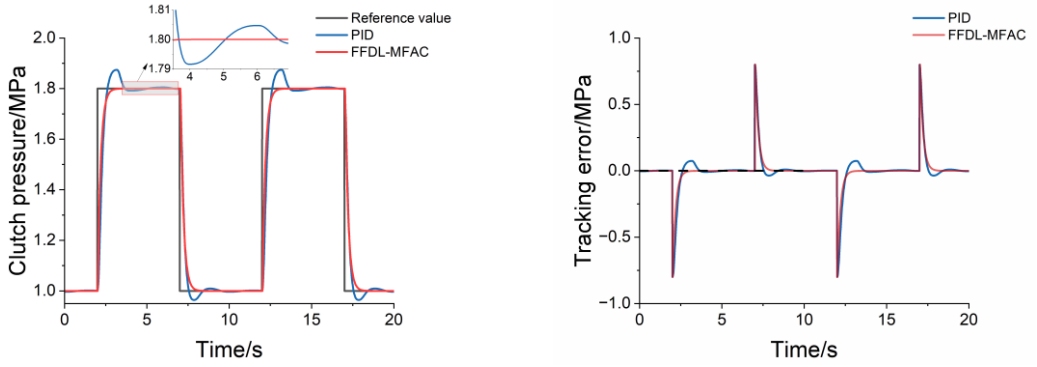

(a) **(b)**

Fig. 7 - Pressure tracking test results under square-wave signal

a) Clutch pressure; b) Pressure tracking error

Sinusoidal pressure tracking test

A 10 s segment of the sinusoidal pressure-tracking experiment was shown in Fig. 8. The reference pressure had an amplitude of 0.465 MPa, an angular frequency of 0.628 rad/s, and a mean level 1.465 MPa. Both PID and FFDL-MFAC controllers were capable of tracking the continuously varying trajectory. The PID controller resulted in a maximum tracking error of 0.036 MPa, accompanied by evident transient deviations around the peak and valley regions and a response delay of approximately 0.07 s. In contrast, the FFDL-MFAC controller reduced the maximum tracking error to 0.021 MPa and exhibited no appreciable delay. These results indicated that the FFDL-MFAC controller substantially mitigates dynamic response lag while preserving high tracking accuracy, thereby demonstrating superior performance under continuously varying pressure trajectories.

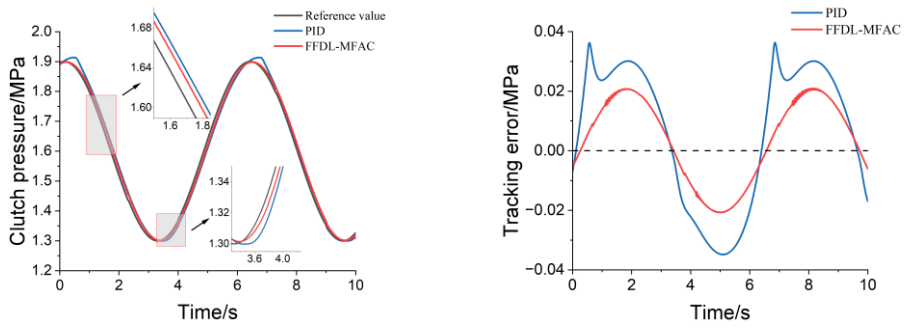

(a) **(b)**

Fig. 8 - Pressure tracking test results under sine-wave signal

a) Clutch pressure; b) Pressure tracking error

Hardware-in-the-loop (HIL) bench test results

To further evaluate controller performance under practical execution conditions, a hardware-in-the-loop (HIL) step-response test was conducted using the real TCU integrated with the high-fidelity hydraulic actuator model, as shown in Fig. 9. In contrast to the co-simulation stage, the HIL setup captured actuator filling delays and the actual computation-to-actuation characteristics of the controller. As a result, it provided a realistic assessment of the transient response, steady-state behavior, and hardware feasibility when the controller is executed on physical electronics. As shown in Fig. 9(a), two tillage load cases were applied, corresponding to moderate and heavy load condition obtained from field measurements in our previous study (*Fu et al., 2025*). The reference pressure increased from 0 MPa to 1.5 MPa in Fig. 9(b).

Under both load conditions, the measured pressure responses throughout the entire clutch pressure control test were nearly identical: the actuator exhibited an inherent filling delay of approximately 0.2 s due to clutch chamber geometry, and the external load exerted negligible influence on the filling dynamics. After filling, the PID controller reached a peak pressure of 1.64 MPa with a 9.44% overshoot, while the FFDL-MFAC controller achieved monotonic rise without overshoot. Using the ±2% tolerance band, the settling times of the PID and FFDL-MFAC controlled systems were 3.12 s and 1.24 s, respectively. In steady state, the PID output exhibited noticeable steady-state fluctuations, while FFDL-MFAC maintained near-zero fluctuation and negligible deviation from the reference. These results confirmed that the filling behavior is largely load-independent and that the proposed controller maintained consistent transient and steady-state performance across different tillage loads.

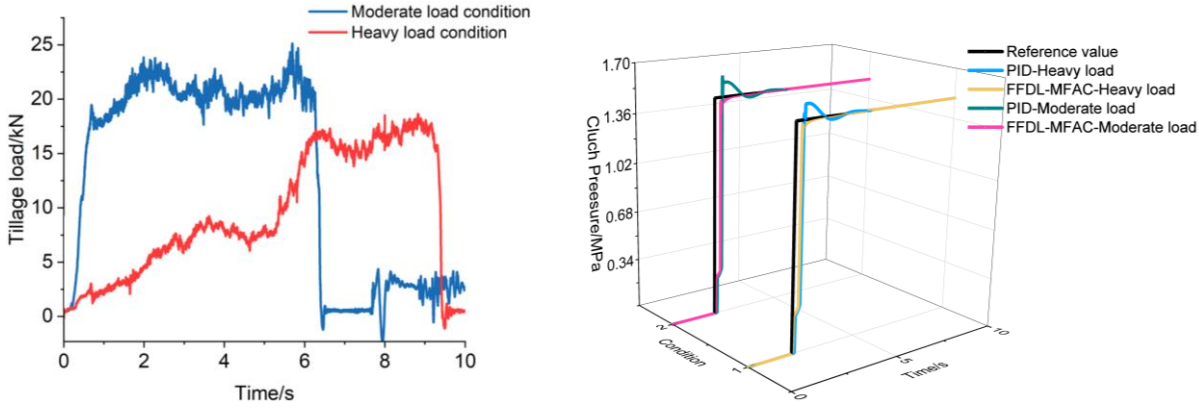

(a) (b)

Fig. 9 - HIL-Based Evaluation of the Clutch Pressure Control Performance

a) tillage load variation; b) Clutch pressure tracking curves

CONCLUSIONS

This study presents an adaptive clutch pressure control method for tractor powershift transmissions based on the FFDL-MFAC algorithm to overcome nonlinearity, strong coupling, and disturbance sensitivity:

(1) A dynamic hydraulic model of the tractor powershift wet clutch was established, and an FFDL-MFAC controller was developed to tackle the strong nonlinearity, parameter time-variation, and significant external disturbances in clutch pressure control. To enhance tuning efficiency, Sobol global sensitivity analysis was applied to identify the key parameters, followed by global optimization using the Improved Mayfly Algorithm (IMA). Co-simulation results showed that the FFDL-MFAC controller achieves markedly superior tracking performance compared with PID control. In square-wave and sinusoidal tests, it reduced rising and falling adjustment times by 72.6% and 59.1%, lowered the maximum tracking error by 41.7%, and shortened the response delay by 92.9%, while maintaining fully monotonic and overshoot-free behavior.

(2) A hardware-in-the-loop (HIL) system was established, and clutch pressure control tests were conducted under two tillage load conditions to evaluate the effectiveness and robustness of the proposed FFDL-MFAC algorithm. The measured pressure responses throughout the entire clutch pressure control test were nearly consistent between the two tillage loads. Under these scenarios, the PID controller produced a 9.44% overshoot, a 3.12 s settling time, and a 0.40 MPa steady-state pressure oscillations. In contrast, the FFDL-MFAC controller eliminated overshoot, reduced the settling time to 1.24 s, and substantially suppressed steady-state fluctuations, demonstrating stable and superior control performance across different tillage depths.

Future work will aim to extend the proposed control strategy to coordinated multi-clutch powershift operation and to evaluate its performance under more complex shifting scenarios.

ACKNOWLEDGEMENT

This research was supported by the project ZR2022QE217 supported by Shandong Provincial Natural Science Foundation.

REFERENCES

[1] Cvok, I., Deur, J., Ivanovic, V., Zhang, Y. J., & Fujii, Y. (2024). Optimal Control Allocation-Based Automatic Transmission Upshift Control Strategy for Inertia Phase. *Ieee Transactions on Vehicular Technology*, *73*(2), 1957-1973. https://doi.org/10.1109/tvt.2023.3321513

[2] Duan, Z., Liu, R., & Liu, C. (2024). 3DDV-Hop node localization optimized based on multi-strategy

improved sparrow search algorithm（多策略改进麻雀搜索算法优化三维 DV-Hop 节点定位）. *Journal of Jilin University(Engineering and Technology Edition)*, *54*(03), 771-784. https://doi.org/10.13229/j.cnki.jdxbgxb.20220530

[3] Feng, H., Ma, W., Yin, C., & Cao, D. (2021). Trajectory control of electro-hydraulic position servo system using improved PSO-PID controller. *Automation in Construction*, *127*, 103722.

[4] Fu, S., Tang, R., Ren, N., Zhang, X., & Lan, R. (2025). Online measurement method for tractor drive wheel slip ratio based on IMA-PKF. *INMATEH-Agricultural Engineering*, *77*(3), 169-180.

[5] Han, L., Liu, H. X., Wang, J. W., Li, S. S., & Ren, L. L. (2019). Optimization Control of CVT Clutch Engagement Based on MPC. *International Journal of Automotive Technology*, *20*(6), 1161-1171. https://doi.org/10.1007/s12239-019-0109-5

[6] Hasan, M. M., Rana, M., Tabassum, F., Pota, H. R., & Roni, M. H. K. (2023). Optimizing the initial weights of a PID neural network controller for voltage stabilization of microgrids using a PEO-GA algorithm. *Applied Soft Computing*, *147*, 110771.

[7] Jung, S., Choi, S. B., Kim, J., Ko, Y., & Lee, H. (2020). Adaptive feed-forward control of the clutch filling phase for wet dual clutch transmission. *IEEE Transactions on Vehicular Technology*, *69*(9), 9577-9588.

[8] Li, A., Qin, D., Guo, Z., Xia, Y., & Lv, C. (2023). Wet clutch pressure hysteresis compensation control under variable oil temperatures for electro-hydraulic actuators. *Control Engineering Practice*, *141*, 105723.

[9] Meng, F., Chen, H. Y., Zhang, T., & Zhu, X. Y. (2015). Clutch fill control of an automatic transmission for heavy-duty vehicle applications. *Mechanical Systems and Signal Processing*, *64-65*, 16-28. https://doi.org/10.1016/j.ymssp.2015.02.026

[10] Mi, B., Huo, X., Ma, K., & Jin, S. (2025). Dynamic Linearization Residual-Assisted Model-Free Adaptive Control With Modified Criterion Function Based on Extended FFDL Data Model. *IEEE Transactions on Industrial Electronics*, *72*(10), 10585-10594.

[11] Song, X., & Sun, Z. (2011). Pressure-based clutch control for automotive transmissions using a sliding-mode controller. *IEEE/ASME transactions on mechatronics*, *17*(3), 534-546.

[12] Walker, P.D., Zhang, N., & Tamba, R. (2011). Control of gear shifts in dual clutch transmission powertrains. *Mechanical Systems and Signal Processing*, *25*(6), 1923-1936.

[13] Wang, D., Zhang, W., JI, J., Dong, Z., Zhu, H., & Li, Z. (2025). Research on the optimization method of clutch engagement trajectory in the tractor power shift process. *INMATEH-Agricultural Engineering*, *75*(1), 35-44.

[14] Xin, Z., Wenjuan, C., Jingtian, L., & Feng, L. (2025). A thrust estimation and control method of an adaptive cycle engine based on improved MFAC algorithm. *Chinese Journal of Aeronautics*, *38*(5), 103424.

[15] Xiong, S., Hou, Z., & Systems, L. (2020). Model-free adaptive control for unknown MIMO nonaffine nonlinear discrete-time systems with experimental validation. *IEEE Transactions on Neural Networks*, *33*(4), 1727-1739.

[16] Yuan, S., Zhang, X., Tan, Y., & Li, Q. (2025). Self-tuning method for optimal control parameters based on adaptive output current（基于输出电流自适应的最优控制参数自整定方法）. *Journal of Electronic Measurement and Instrumentation*, *39*(07), 54-62.

[17] Zhang, C., Yu, H., Shi, W., Liu, Q., Hong, J., & Gao, B. (2022). Nonlinear Pressure Control of Electronically Controlled Hydraulic Direct Drive Multi-Disc Clutch（电控液压直驱多片离合器非线性压力控制）. *Transactions of Beijing Institute of Technology*, *42*(08), 850-856. https://doi.org/10.15918/j.tbit1001-0645.2021.199

[18] Zhao, J., Xiao, M.H., Bartos, P., & Bohata, A. (2021). Dynamic engagement characteristics of wet clutch based on hydro-mechanical continuously variable transmission. *Journal of Central South University*, *28*(5), 1377-1389.

[19] Zhao, N.-c., Che, G., Wan, L., Zang, S., Wu, C.-s., & Guo, Z.-j. (2025). Design and Test of Path Tracking Control System for Soybean Weeding Robot. *INMATEH-Agricultural Engineering*, *77*, 1532-1542. https://doi.org/10.35633/inmateh-77-122

[20] Zhou, B., Zhang, J., Gao, J., Yu, H., & Liu, D. (2018). Clutch pressure estimation for a power-split hybrid transmission using nonlinear robust observer. *Mechanical Systems and Signal Processing*, *106*, 249-264.

[21] Zhu, Y., & Hou, Z. (2013). Data-driven MFAC for a class of discrete-time nonlinear systems with RBFNN. *IEEE Transactions on Neural Networks and Learning Systems*, *25*(5), 1013-1020.